Supporting Information

Wang et al. 10.1073/pnas.1120380109

SI Materials and Methods

Slice Preparation and Surgery. All slice experiments used cerebellum from 14- to 23-d-old Sprague-Dawley rat pups or C57BL/6 mouse pups (Charles River). Transgenic mice [inositol 1,4,5-trisphosphate (IP_3) receptor subtype 2 knockout mice ($IP_3R2^{-/-}$) or $MrgA1^+$] were cross-bred with C57/BL6 for at least five generations (1). Slices (350 μm thick) and solutions were prepared as previously described (2).

For in vivo experiments, adult C57BL/6 mice (25–30 g; Charles River), reporter mice expressing EGFP under the glutamate transporter 1 (GLT1) promoter (GLT1-EGFP), $IP_3R2^{+/+}$ and $IP_3R2^{-/-}$ littermates, or $MrgA1^+$ mice (1, 3) were anesthetized with ketamine (60 mg/kg) and xylazine (10 mg/kg) and ventilated (SAR-830; CWE) through a tracheal cannula. A femoral artery was cannulated for monitoring of blood gases. A craniotomy was made over the cerebellar vermis for bolus-loading of the Ca^{2+} indicator rhod2/am (4), two-photon imaging (5), recording of cerebellar electrocortical activity (ECoG) (6), and extracellular K^+ measurement (7, 8).

All animal experiments were conducted in accordance with the guideline of the Animal Care and Use Committee of the University of Rochester.

Electrophysiology. Bergmann glial cells were recognized by their lack of action potentials upon injection of depolarizing current and by their small somata (~10 μm) compared with the large cell bodies of Purkinje neurons (30 to ~40 μm). All recordings in both Purkinje cells and Bergmann glial cells were obtained in a depth of 80–100 μm below the surface of the slice. Membrane potentials were recorded under current–clamp with an Axopatch MultiClamp 700B amplifier (Axon Instruments). No currents were injected ($I = 0$) unless indicated. Data were low-pass–filtered at 2 kHz and digitized at 10 kHz with a Digidata 1440 interface controlled by pCLAMP software (Molecular Devices). Patch electrodes with a resistance of 3–5 MΩ and 6–9 MΩ were used for patching Purkinje cells and Bergmann glia, respectively, whereas pipettes with a resistance of 7–12 MΩ were used for cell-attached or extracellular recording (2). For in vivo ECoG recordings, the electrodes were filled with artificial cerebrospinal fluid (aCSF), inserted ~80–100 μm below the cerebellar surface, and then filtered from 1 to 100 Hz (9). For in vivo experiments, the agonists Phe-Met-Arg-Phe amide (FMRF; 15 μM) in $MrgA1^+$ mice or ATP (100 μM) in GLT1-EGFP mice were added to aCSF and perfused over the exposed vermis.

Two-Photon Laser Scanning Microscopy. A custom-built microscope attached to a Tsunami/Millenium laser (10 W; Spectra-Physics) and scan box (FV300; Olympus) using FluoView software was used for two-photon laser scanning microscopy. Most experiments used a 40× objective (0.9 N.A.; Olympus). Excitation wavelength was 820–840 nm. Two-channel detection of emission wavelength was achieved by using a 565-nm dichroic mirror (Chroma) and two external photomultiplier tubes. A 525/50 bandpass filter (Chroma) was used to detect Alexa Fluor 488, and a 620/60 bandpass filter (Chroma) was used to detect rhod2 emission wavelengths. In slice experiments, rhod2/am was dissolved in DMSO with 20% (mol/vol) Pluronic F-127 and mixed with aCSF. Slices were incubated with 10 μM rhod2/am for 30–60 min.

For in vivo imaging experiments, 50 μg of rhod2/am was dissolved in 10 μL of DMSO containing 20% (mol/vol) Pluronic F-127. The solution was diluted 1:8 in aCSF. The dye solution was delivered with a micropipette (resistance 2–3 MΩ) inserted ~80 μm deep into the vermis by pressure (50–500 mbars) with a Picospritzer III (Parker). The two-photon laser power was less than 30 mW.

K^+-Sensitive Microelectrodes. Ion-sensitive microelectrodes were fabricated from double-barreled pipette glass (PB150F-6; WPI) pulled to a tip of <3 μm with a puller (P-97; Sutter). The pipette was silanized by dimethylsilane (Fluka; Sigma) loaded with a 100- to 150-μm column of valinomycin-based K ion-exchanger resin (potassium ionophore 1, mixture B, Fluka; Sigma) and backfilled with 150 mM KCl. The reference barrel was filled with Hepes-buffered 150 mM NaCl solution (pH = 7.4). Electrodes were calibrated in 1–6 mM K^+ in aCSF before and after experiments and displayed voltage responses of 5–6 mV per mM increase in K^+ concentrations (7, 8).

Analysis. Analysis of data was performed with Clampfit 10 software (Axon Instruments) and SigmaStat 3.0 (SPSS). Distributions of up and down states were constructed by using histograms of membrane potential distribution. To measure the duration of up state, the membrane potential with the lowest value between the two states was taken as the transition point. Time above and below the transition point was added and expressed as a percentage of the whole. The 1 min of recordings before and after application of drugs were analyzed for histograms of membrane potential and time distribution, unless noted otherwise. Interspike intervals (ISIs) for whole-cell recording were obtained by using Template Search in Clampfit 10.2 software. Clampfit 10.2 software was used for power spectrum analysis of in vivo ECoG recordings. Three 20-s ECoG epochs before, during, and after agonist exposure were analyzed.

1. Holtzclaw LA, Pandhit S, Bare DJ, Mignery GA, Russell JT (2002) Astrocytes in adult rat brain express type 2 inositol 1,4,5-trisphosphate receptors. *Glia* 39:69–84.
2. Li X, Zima AV, Sheikh F, Blatter LA, Chen J (2005) Endothelin-1-induced arrhythmogenic Ca^{2+} signaling is abolished in atrial myocytes of inositol-1,4,5-trisphosphate(IP3)-receptor type 2-deficient mice. *Circ Res* 96(12):1274–1281.
3. Kang J, Jiang L, Goldman S, Nedergaard M (1998) Astrocyte-mediated potentiation of inhibitory synaptic transmission. *Nature neuroscience* 1(8):683–692.
4. Ohki K, Chung S, Ch'ng YH, Kara P, Reid RC (2005) Functional imaging with cellular resolution reveals precise micro-architecture in visual cortex. *Nature* 433(7026):597–603.
5. Wang X, et al. (2006) Astrocytic $Ca^{(2+)}$ signaling evoked by sensory stimulation in vivo. *Nature neuroscience* 9:816–823.
6. Spasic S, et al. (2008) Spectral and fractal analysis of cerebellar activity after single and repeated brain injury. *Bull Math Biol* 70(4):1235–1249.
7. Hounsgaard J, Nicholson C (1983) Potassium accumulation around individual Purkinje cells in cerebellar slices from the guinea-pig. *J Physiol* 340:359–388.
8. Nedergaard M, Hansen AJ (1993) Characterization of cortical depolarizations evoked in focal cerebral ischemia. *J Cereb Blood Flow Metab* 13(4):568–574.

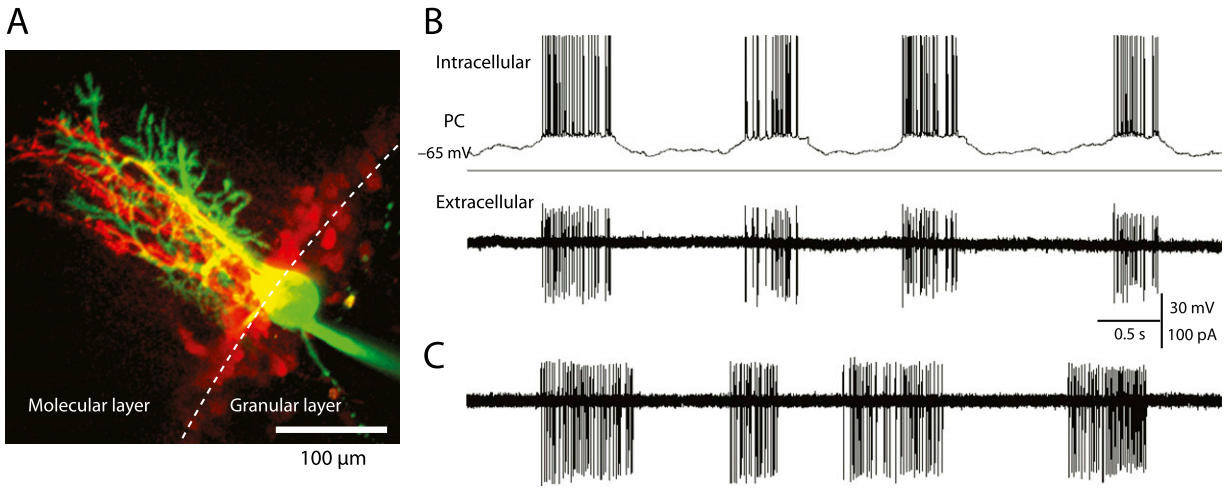

Fig. S1. Extracellular recordings of Purkinje cell (PC) activity detect periodic fluctuations in the membrane potential between two preferred states: up state (depolarized) and down state (hyperpolarized). (*A*) An image of a Bergmann glial cell filled with Alexa Fluor 594 (red) and an adjacent Purkinje cell filled with Alexa Fluor 488 (green) via patch electrode. (Scale bar: 100 μm.) (*B*) Whole-cell recording (intracellular) from a Purkinje cell (upper trace) combined with extracellular recording (lower trace) shows that action potentials can be consistently detected as simple spikes in the extracellular recordings. (*C*) Extracellular recording only show that Purkinje cell bistability is not an artifact of intracellular recordings because they are present in the absence of intracellular recordings.

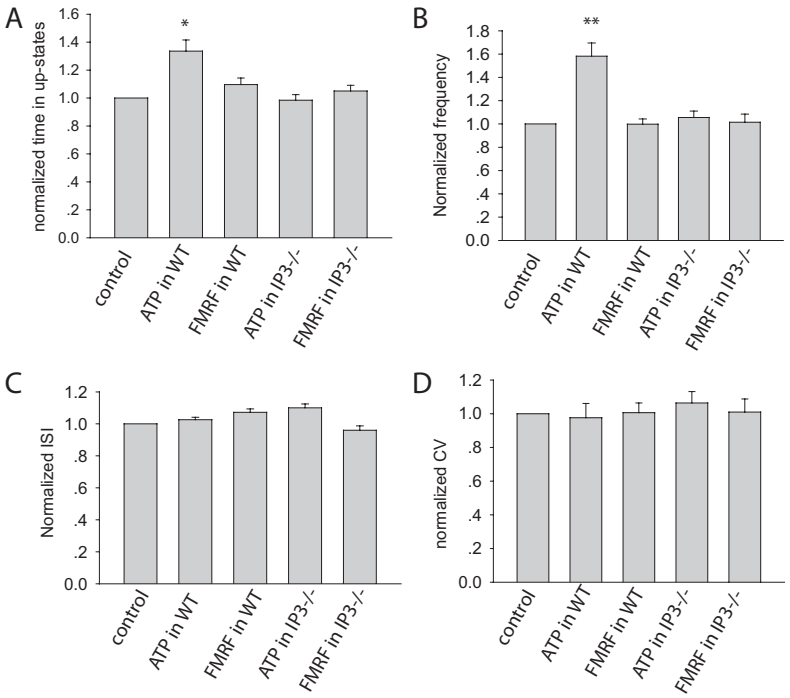

Fig. S2. Control experiments showing the effects of application of FMRF (15 μM) and ATP (100 μM) on the relative time spent in up state and frequency of action potentials in WT mice and in $IP_3^{-/-}$ mice. (*A*) Comparison of relative time in up state (*$P < 0.05$, one-way ANOVA, $n = 5–7$). (*B*) Comparison of the frequency of action potentials (**$P < 0.01$, one-way ANOVA, $n = 5–7$) (*C* and *D*) Comparison of the ISIs (*C*) and coefficients of variance (CVs) (*D*) of action potentials on up states in the same groups.

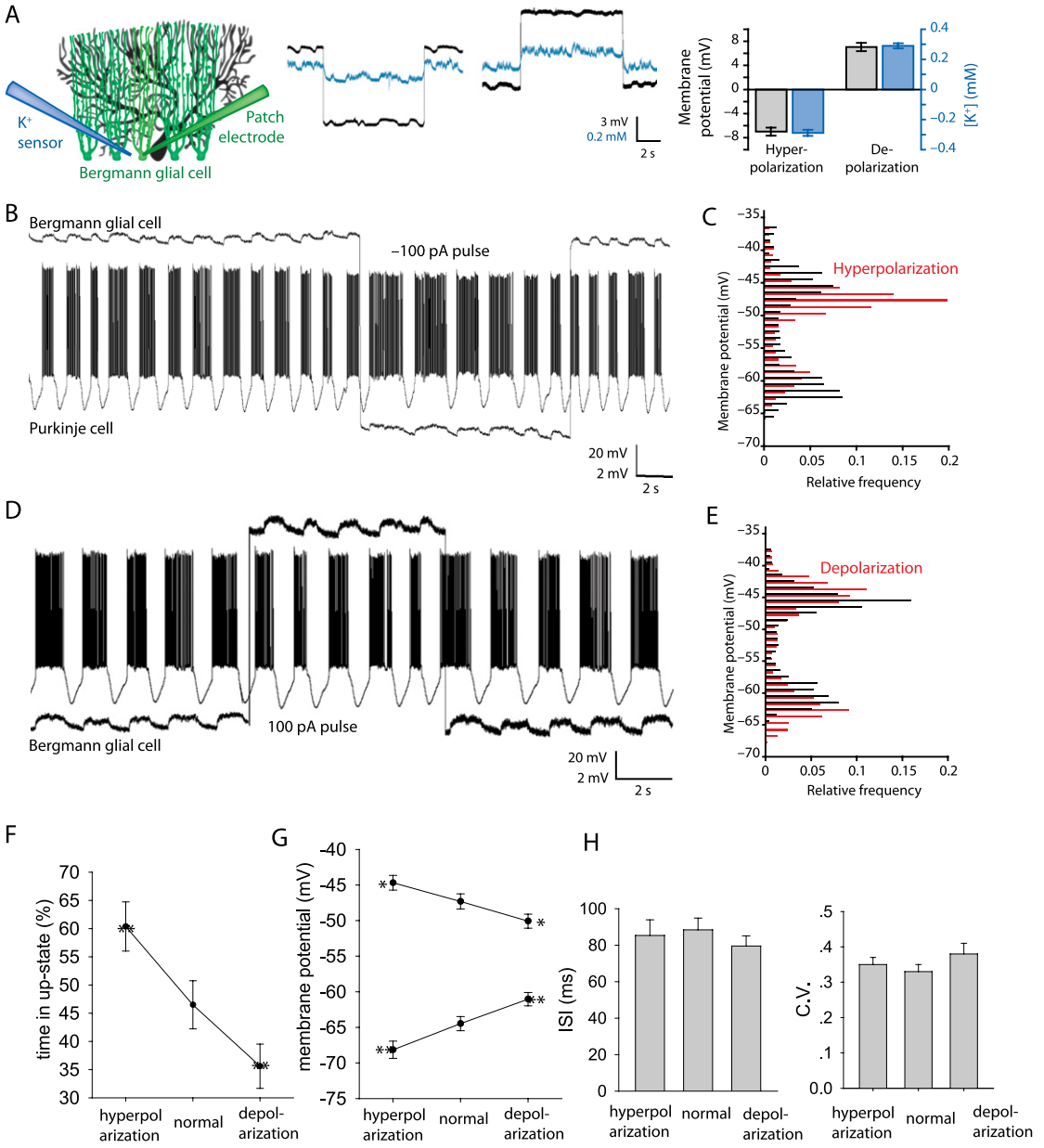

Fig. S3. Hyper- or depolarization of Bergmann glial cells changes extracellular K^+ and Purkinje cell bistability. (*A*) Combining whole-cell recording of Bergmann glial cells with recording of extracellular K^+. Hyperpolarization (100 pA) decreased the membrane potential of Bergman glial cells by −7.04 ± 0.69 mV (n = 6) and lowered extracellular K^+ by −0.28 ± 0.02 mM (n = 6). Depolarization hyperpolarized the membrane potential of Bergmann glial cells by 7.00 ± 0.68 mV (n = 6) and increased the extracellular K^+ by 0.28 ± 0.02 mM (n = 6). (*B*) Dual whole-cell recording of Purkinje cells and Bergmann glial cells. Hyperpolarization of the Bergmann glial cell increases the time spent in up state. (*C*) Histogram shows the corresponding membrane potential distribution for *B*. (*D*) Depolarization caused a decrease in up state. (*E*) Histogram shows the corresponding membrane potential distribution for *D*. (*F*) Histogram shows the changes of time in up states in Purkinje cells induced by hyper- and depolarization of Bergman glial cells (**P < 0.01, one-way ANOVA, n = 6). (*G*) Histogram shows the changes of membrane potentials in Purkinje cells induced by hyper- and depolarization of Bergman glial cells (*P < 0.05, **P < 0.01, one-way ANOVA, n = 6). (*H*) Histogram shows the ISIs and CVs of action potentials in Purkinje cells induced by hyper- and depolarization of Bergman glial cells.

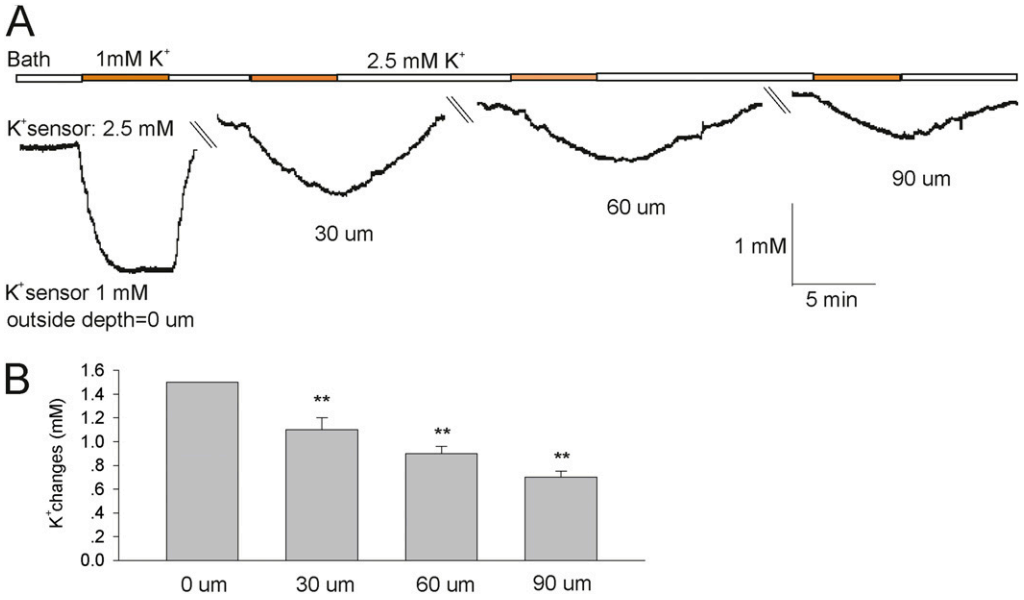

Fig. S4. Changes of extracellular K^+ in response to repeatedly changing bath K^+ from 2.5 mM to 1.0 mM and back. (*A*) A typical recording of K^+ at different depth of tissue, when switching bath solution from 2.5 mM to 1.0 mM for 5 min and back. The gaps in the trace were the noises when we changed the depth of the electrode. (*B*) Comparison of the peak changes of K^+ observed after the 3-min changes of bath K^+ (**$P < 0.01$, one-way ANOVA, $n = 5$).

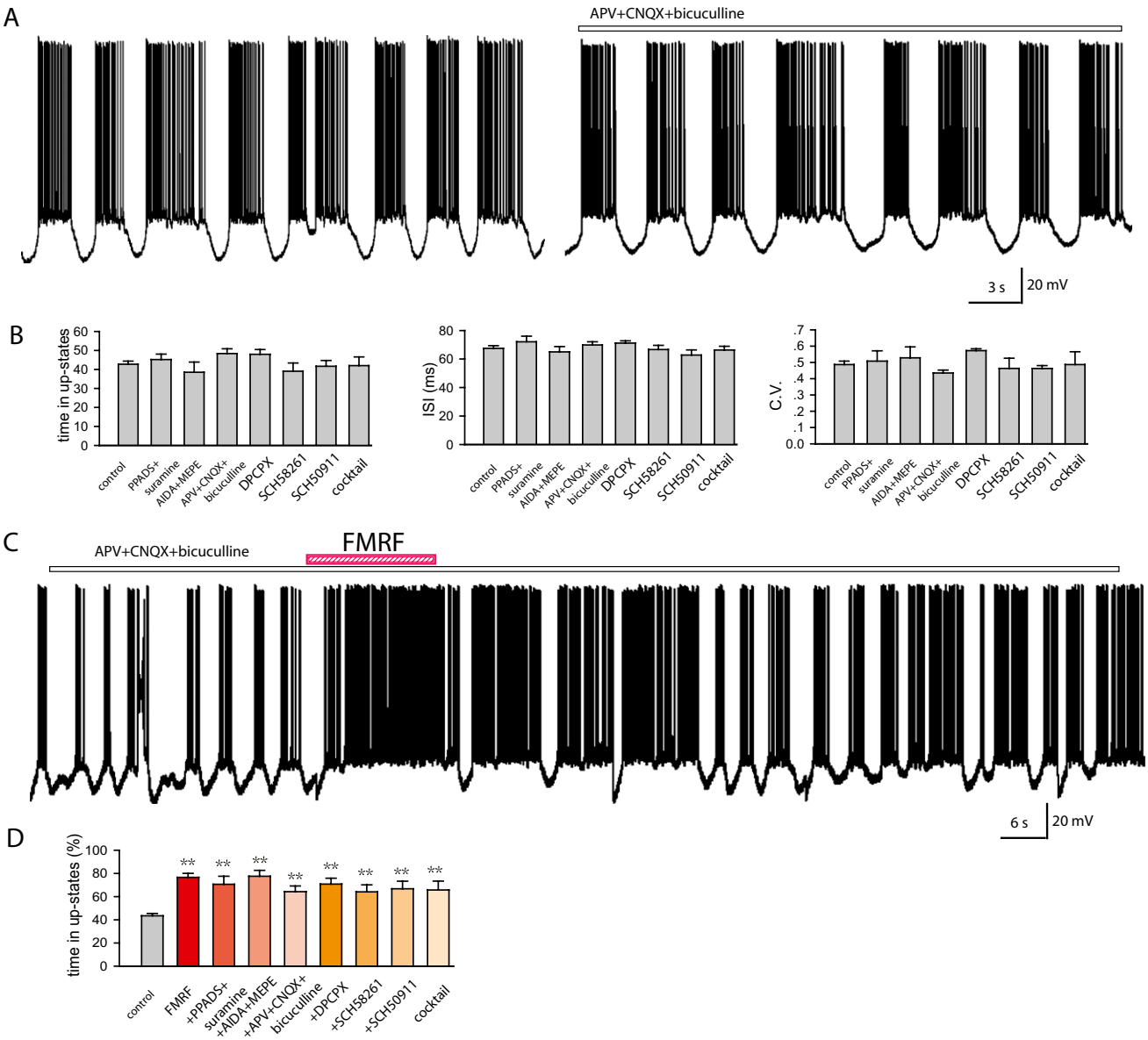

Fig. S5. The effects of FMRF on Purkinje cell bistability were insensitive to an array of receptor antagonists. (*A*) Representative recording from a Purkinje cell before and after addition of AP5 (20 μM), 6-cyano-7-nitroquinoxaline-2,3-dione (CNQX; 5 μM), and bicuculline (2 μM). (*B*) Comparison of time spent in up state, ISI, and CV in controls and slices exposed to AP5/CNQX/bicuculline, pyridoxal-phosphate-6-azophenyl-2′,4′-disulfonate (PPADS; 10 μM)/Suramin (5 μM), (*RS*)-1-aminoindan-1,5-dicarboxylic acid (AIDA; 20 μM)/2-methyl-6-(phenylethynyl)-pyridine hydrochloride (MPEP; 10 μM), or 8-cyclopentyl-1,3-dipropylxanthine (DPCPX; 300 nM), SCH50911 (10 μM), and SCH58261 (1 μM) (n = 5–20). (*C*) Representative trace of slice (from MrgA1$^+$ mouse) exposed to FMRF in the presence of AP5/CNQX/bicuculline. (*D*) Comparison of time spent in up state during FMRF exposure in slices prepared from MrgA1$^+$ mice and those in the presence of the antagonists AP5/CNQX/bicuculline, PPADS (10 μM)/Suramin (5 μM), AIDA (20 μM)/MPEP (10 μM), DPCPX (300 nM), SCH50911 (10 μM), SCH58261 (1 μM), or a mixture of all of the antagonists in the same concentration as tested individually (n = 5–21, $^*P < 0.05$, $^{**}P < 0.01$).